Research Article | Vol. 27, No. 9 | 29 Apr 2019 | OPTICS EXPRESS 12137
Optics EXPRESS

Wavelength modulation spectroscopy by employing the first harmonic phase angle method

CHENGUANG YANG,[1] LIANG MEI,[2] HAO DENG,[1] ZHENYU XU,[1] BING CHEN,[1] AND RUIFENG KAN[1,3,*]

[1]*Key Laboratory of Environmental Optics and Technology, Anhui Institute of Optics and Fine Mechanics, Chinese Academy of Science, Hefei 230031, China*
[2]*School of Optoelectronic Engineering and Instrumentation Science, Dalian University of Technology, Dalian 116024, China*
[3] *State Key Laboratory of Applied Optics, Changchun Institute of Optics, Fine Mechanics and Physics, Chinese Academy of Sciences, Changchun 130033, China*
** rfkan@ciomp.ac.cn*

Abstract: Wavelength modulation spectroscopy (WMS), widely employed in tunable diode laser absorption spectroscopy (TDLAS), has been accomplished by employing the first harmonic phase angle (1*f*-PA) method that is immune to the laser intensity and the demodulation phase. The principle of the 1*f*-PA method has been demonstrated by the phasor decomposition method, which indicates that the 1*f*-PA is linearly proportional to the integral absorption in the approximation of weak absorption. Validation experiments have been performed to investigate the relationship between the 1*f*-PA and the modulation amplitude/frequency by measuring the absorption line of CO_2 around 6362.5 cm^{-1}. The peak-to-peak value of the 1*f*-PA decreases with the increasing of the modulation amplitude, and is particularly apparent under small modulation amplitudes and high modulation frequencies. The 1*f*-PA shows good linearity with the increasing of the CO_2 concentration. Comparing with the traditional first harmonic normalized second harmonic (2*f*/1*f*) method, higher detection sensitivities can be achieved at high modulation frequencies. The promising results imply that the 1*f*-PA method has a great potential in the applications of the WMS technique especially under high modulation frequencies or modulation-amplitude limited conditions, such as strong turbulence or high pressure environments.

1. Introduction

As the rapid development of infrared diode laser technologies, tunable diode laser absorption spectroscopy (TDLAS) technology has been widely applied in greenhouse gas and air pollution monitoring, combustion diagnostics, industrial processes control, etc [1–6]. Traditionally, there are mainly two different approaches to accomplish the TDLAS technology, namely the direct absorption spectroscopy (DAS) [5] that recovers the absorption line-shape by scanning the laser wavelength across the absorption peak of the target gas, and the wavelength modulation spectroscopy (WMS) [6] that detects the gas absorption harmonics by scanning and modulating the laser frequency simultaneously. The WMS technique can greatly improve the detection sensitivity up to 10^{-5}-10^{-6} $Hz^{-1/2}$ as the 1/*f* noise is significantly suppressed by shifting the detection band to high frequency [2]. During the past decades, the WMS technique has been extensively employed as an effective tool for high-sensitivity gas sensing [7–21].

In the WMS technique, the second harmonic (2*f*) signal is often employed for gas concentration retrieval [8–13]. In order to eliminate the dependency on the laser power, Hanson et al. [9,10] utilized the first harmonic normalized second harmonic (2*f*/1*f*) signal for gas concentration retrieval based on the quadrature demodulation method. In order to achieve

#359580 https://doi.org/10.1364/OE.27.012137
Journal © 2019 Received 6 Feb 2019; revised 27 Mar 2019; accepted 3 Apr 2019; published 17 Apr 2019

Optics EXPRESS

the maximize signal intensity, the optimized modulation index (*m*), which is the ratio between the frequency modulation (FM) amplitude and the half-width at half-maximum (HWHM) of the absorption feature, should be equal to about 2.2 for 2*f* signal [9] and 1.1 for 2*f*/1*f* signal [10]. In high pressure conditions, where the absorption profile will be greatly broadened, large FM amplitude is thus required to achieve the optimum modulation index for the 2*f* method, which can cause strong nonlinear laser response and increase the complexity of signal analysis [11]. In strong turbulence or high time-resolution measurements, requiring high modulation frequencies, large FM amplitude is very difficult to achieve due to the limited FM response ratio of laser diodes [12]. Thus, the optimum modulation index for the 2*f* method is very difficult to achieve in extreme conditions due to the limitations on the injection current of laser diodes.

In this work, a gas concentration retrieval approach based on the first harmonic phase angle (1*f*-PA) method, which is immune to the laser power and the demodulation phase, has been developed and validated. The relationship between the 1*f*-PA of WMS and the gas absorption is, to our knowledge, for the first time investigated. Theoretical analysis as well as numerical simulation has been carried out and the phenomenological explanation is given by the phasor decomposition method. Moreover, the 1*f*-PA method has been studied experimentally by measuring carbon dioxide (CO_2) absorption line around 6362.5 cm^{-1}, and the inter-comparison between the traditional 2*f*/1*f* method and the 1*f*-PA method has also been performed.

2. Principles of the 1*f*-PA method

As mentioned in several early studies [13–16], WMS adds the high-frequency modulation current on the linearly increased injection current of the diode laser, which causes the modulations of the light intensity (I_0) as well as the frequency (ν) simultaneously

$$I_0 = \bar{I}_0\left(1 + i_1\cos\left(2\pi f_m t + \psi\right)\right), \tag{1}$$

$$\nu = \nu_0 + \nu_1\cos\left(2\pi f_m t\right). \tag{2}$$

Here f_m is the modulation frequency, $\bar{I}_0$ and ν_0 are the average laser intensity and the center frequency, i_1 is the relative intensity modulation (IM) amplitude (normalized by $\bar{I}_0$), ν_1 is the relative frequency modulation (FM) amplitude, ψ is the phase shift between the IM and the FM (IM-FM phase shift).

According to the Beer-Lambert Law, the transmitted laser intensity *I* can be expressed as

$$I \approx I_0\left(1-\alpha\right) \approx \bar{I}_0\left(1 + i_1\cos\left(2\pi f_m t + \psi\right) - \alpha\left(\nu\right) - i_1\cos\left(2\pi f_m t + \psi\right)\alpha\left(\nu\right)\right). \tag{3}$$

The absorption coefficient α(ν) can be expanded in the Fourier cosine series

$$\alpha\left(\nu\right) = \alpha\left(\nu_0 + \nu_1\cos\left(2\pi f_m t\right)\right) = \sum_{k=0}^{\infty} H_k\left(\nu_0, \nu_1\right)\cos\left(2\pi k f_m t\right). \tag{4}$$

Here H_k is the k^{th} order Fourier coefficient of absorption, given by

$$\left.\begin{aligned} H_0\left(\nu_0,\nu_1\right) &= \frac{1}{2\pi}\int_{-\pi}^{\pi}\alpha\left(\nu_0 + \nu_1\cos\theta\right)\mathrm{d}\theta \\ H_k\left(\nu_0,\nu_1\right) &= \frac{1}{\pi}\int_{-\pi}^{\pi}\alpha\left(\nu_0 + \nu_1\cos\theta\right)\cos\left(k\theta\right)\mathrm{d}\theta \end{aligned}\right\}. \tag{5}$$

Optics EXPRESS

Demodulating the transmitted laser intensity with the in-phase reference signal and the out-of-phase reference signal, the first harmonic absorption (1*f*) signals, namely X_{1f} and Y_{1f}, can be described by

$$\left.\begin{aligned} X_{1f} &= \frac{\bar{I}_0}{2}\left(i_1\cos\psi - H_1 - i_1H_0\cos\psi - \frac{1}{2}i_1H_2\cos\psi\right) \\ Y_{1f} &= -\frac{\bar{I}_0}{2}\left(i_1\sin\psi - i_1H_0\sin\psi + \frac{1}{2}i_1H_2\sin\psi\right) \end{aligned}\right\}. \tag{6}$$

The first harmonic phase angle (1*f*-PA), denoted as θ_{1f}, can be described by

$$\theta_{1f} = \arctan\left(\frac{Y_{1f}}{X_{1f}}\right) = \arctan\left(\tan(-\psi)\frac{1 - H_0 + \frac{1}{2}H_2}{1 - \frac{1}{i_1\cos(-\psi)}H_1 - H_0 - \frac{1}{2}H_2}\right). \tag{7}$$

As shown in Eq. (7), θ_{1f} is the function of the Fourier coefficients of absorption (H_k), relative IM amplitude (i_1) and the IM-FM phase shift (ψ), but is independent of the laser average intensity $\bar{I}_0$. The background 1*f*-PA without any absorption equals to $-\psi$.

As illustrated in Fig. 1(a), the 1*f*-PA has the similar shape with the first derivative of the gas absorption curve. The waveform distortion of the 1*f*-PA increases with the increasing of the integral absorbance. The linearity between the 1*f*-PA and the integral absorbance is beyond 0.998 with an integral absorbance in the region from 10^{-4} to 0.1, as shown in Fig. 1(b).

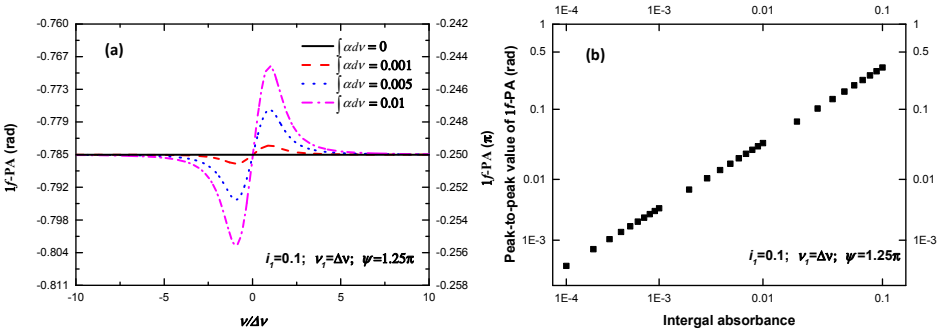

Fig. 1. 1*f*-PA with different integral absorbances (a) and the relationship between the integral absorbance and the peak-to-peak value of 1f-PA (b). FM amplitude (v_1) is supposed to be equal to the absorption half width. The IM-FM phase shift (ψ) is supposed to be 1.25π.

In order to better illustrate the 1*f*-PA, the harmonic signals is further analyzed by the phasor decomposition method [17–21]. According to Eq. (6), the first harmonic signal vector $\vec{R}_{1f}$, consisting of the X_{1f} and Y_{1f}, can be expressed as the sum of a series of vectors, as shown in Fig. 2.

$$\vec{R}_{1f} = R_{1f}e^{i\theta_{1f}} = \frac{\bar{I}_0}{2}i_1e^{i(-\psi)} + \frac{\bar{I}_0}{2}H_1e^{i\pi} + \frac{\bar{I}_0}{2}i_1H_0e^{i(\pi-\psi)} + \frac{\bar{I}_0}{2}i_1H_2e^{i(\pi+\psi)}. \tag{8}$$

The background subtracted 1*f*-PA, namely $\theta_{1f\text{-}0}$, which is the angle difference between the 1*f* signal vector $\vec{R}_{1f}$ and the 1*f* RAM vector $\bar{I}_0i_1e^{i(-\psi)}/2$ is dependent on the absorption and equals to zero under the circumstance of no absorption. As can be seen from Eq. (8), the

Optics EXPRESS

average laser intensity ($\bar{I}_0$) appears in all vectors, which implies that the background subtracted 1*f*-PA ($\theta_{1f\text{-}0}$) is independent of $\bar{I}_0$. As shown in Fig. 3(a), the 1*f* signal vector can be decomposed to X_{1f} and Y_{1f}. The background subtracted 1*f*-PA ($\theta_{1f\text{-}0}$) is independent of the demodulation reference phase.

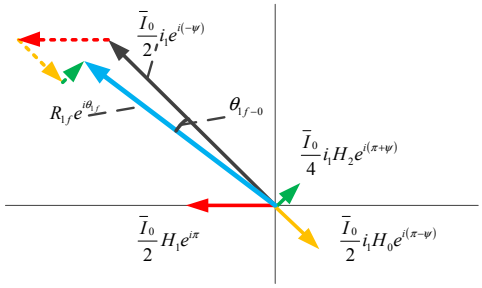

Fig. 2. Phasor diagram of 1*f* signal vector with the coordinate axes in-phase with the FM response. The IM-FM phase shift (ψ) varies from π to 1.5π.

The approximate linear relationship between the background subtracted 1*f*-PA ($\theta_{1f\text{-}0}$) and the integral absorbance for weak absorption can be explained by Fig. 3(b). The absorption-related vectors, $\bar{I}_0 H_1 e^{i(-\pi)}/2$, $\bar{I}_0 i_1 H_0 e^{i(\pi-\psi)}/2$ and $\bar{I}_0 i_1 H_2 e^{i(\pi+\psi)}/4$, are linearly proportional to the integral absorbance and much smaller than the 1*f* RAM vector $\bar{I}_0 i_1 e^{i(-\psi)}/2$. Thus, the sum of these absorption-related vectors has the same properties. As a result, the modulus of the 1*f* signal vector (R_{1f}) approximately equals to the modulus of the 1*f* RAM vector ($\bar{I}_0 i_1/2$), and the background subtracted 1*f*-PA ($\theta_{1f\text{-}0}$) can be approximately estimated by the ratio between the modulus of the sum of these absorption-related vectors and the modulus of the 1*f* RAM vector, which is linearly dependent on the integral absorbance.

As the contribution of the nonlinear response of the diode laser is much smaller than the 1*f* RAM vector $\bar{I}_0 i_1 e^{i(-\psi)}/2$ and other absorption-related vectors in Eq. (8) [9,11], the nonlinear amendment of 1*f*-PA would not affect the properties of this method.

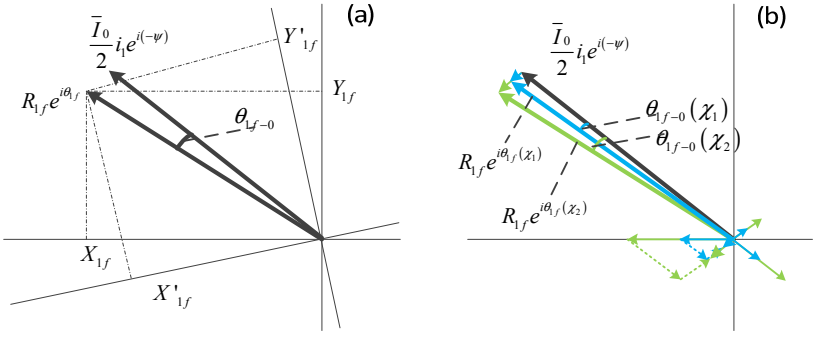

Fig. 3. Phasor analysis of the 1*f* signal vector: (a) decomposition of the 1*f* vector in different coordinate system and (b) 1*f* vector with different integral absorbance.

3. Experiments and results

3.1 Experimental setup

Absorption measurement of CO_2 has been carried out to verify the feasibility and performance of the 1*f*-PA method. The diagram of the experiment setup is shown in Fig. 4. The absorption line of CO_2 at 6362.498 cm^{-1} and several other nearby but relatively weaker absorption lines are chosen to compare the 1*f*-PA method with the traditional 2*f*/1*f* method.

Optics EXPRESS

An 100 Hz, 1.4 V_{pp} (peak-to-peak voltage) sawtooth signal plus a sine wave, generated by the multifunction I/O device (NI Corporation, USB-6363) with 2 MS/s sample rate, is sent to a homemade laser controller to drive the near infrared DFB diode laser (NTT, NLK1L5EAAA). The bandwidth of the homemade laser controller is 2 MHz, which is much higher than the upper limit (100 kHz) of the modulation frequency in the following experiments. The laser beam is divided by the fiber splitter into two parts, the measurement path and the reference path. The measurement path is addressed to the 50 cm gas cell and the transmitted laser beam is detected by a photodiode (PD1, Thorlabs, PDA20CS-EC). The detected signal is acquired by the same multifunction I/O device mentioned above with 2 MS/s sample rate. The reference signal detected by the other photodiode (PD2, Thorlabs, PDA10DT-EC) is acquired by an oscilloscope. The free spectral range of the homemade quartz etalon is 0.0173 cm^{-1}. The limited vacuum and vacuum leak rate of the gas cell are 280 Pa and 5 Pa/h, respectively. The pressure in the gas cell is controlled at the near atmosphere pressure (105500 ± 500 Pa) by the metering valve.

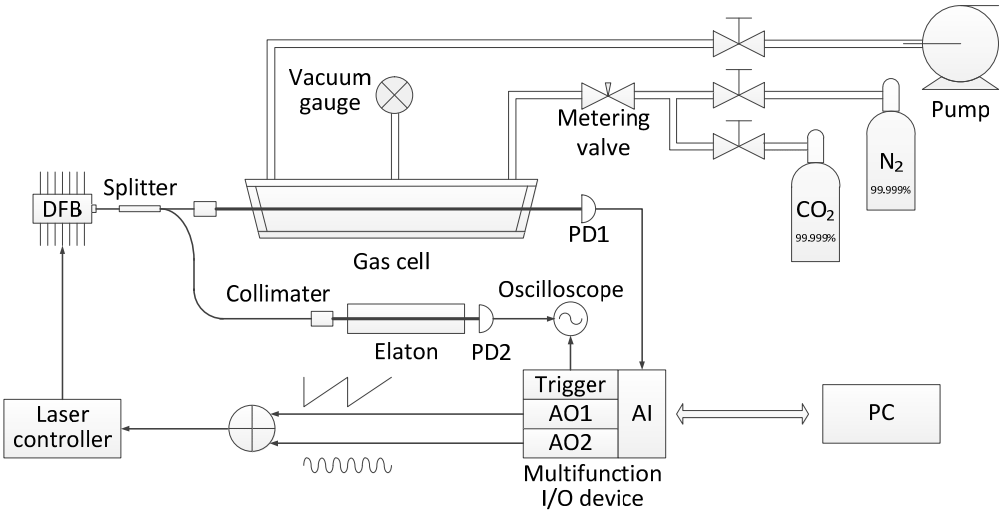

Fig. 4. Diagram of the experiment setup for the first harmonic detection. DFB-distributed feedback diode laser, AO-Analog Output, AI-Analog Input, PD-photo diode, PC-Personal Computer

3.2 First harmonic phase angle signal

Figure 5 shows the experimental results measured with pure CO_2 and pure N_2. The frequency and amplitude of the modulation signal are 30 kHz and 350 mV corresponding to 28 mA modulation current, respectively. The laser FM amplitude, measured by the etalon, equals to 0.1038 cm^{-1}. The modulation index m is 1.059 for 1 atm pure CO_2. The quadrature 1f signals of absorption (X_{1f}, Y_{1f}) and background (X^0_{1f}, Y^0_{1f}), shown in Fig. 5(c), are obtained by digitally demodulating the original signals (Figs. 5(a) and 5(b)) with 2 kHz low-pass filter and arbitrary demodulation phase, i.e., 0° in this case. As can be seen in Fig. 5(d), the absorption 1f-PA (θ_{1f}) has explicit waveform distortions around the absorption peaks, while the background 1f-PA (θ^0_{1f}) is nearly a straight line. The background subtracted 1f-PA ($\theta_{1f\text{-}0}$) is a baseline-free curve with phase distortions only around the absorption peaks.

As shown in Fig. 6, the peak and valley of the absorption and the background 1f-PAs periodically change as the demodulation phase varies from 0° to 360°. Except the hopping of the 1f-PA signal at 30°, 40°, 210° and 220° demodulation phase due to the arc-tangent function, the peak-to-peak values of the 1f-PA (θ_{1f}) and the background subtracted 1f-PA ($\theta_{1f\text{-}0}$) remain unchanged in this case, i.e., 0.344 rad and 0.343 rad, respectively. In order to reduce

Optics EXPRESS

the phase jitter and baseline due to the arbitrary demodulation phase, the background subtracted 1*f*-PA ($\theta_{1f\text{-}0}$) will be used in the following section.

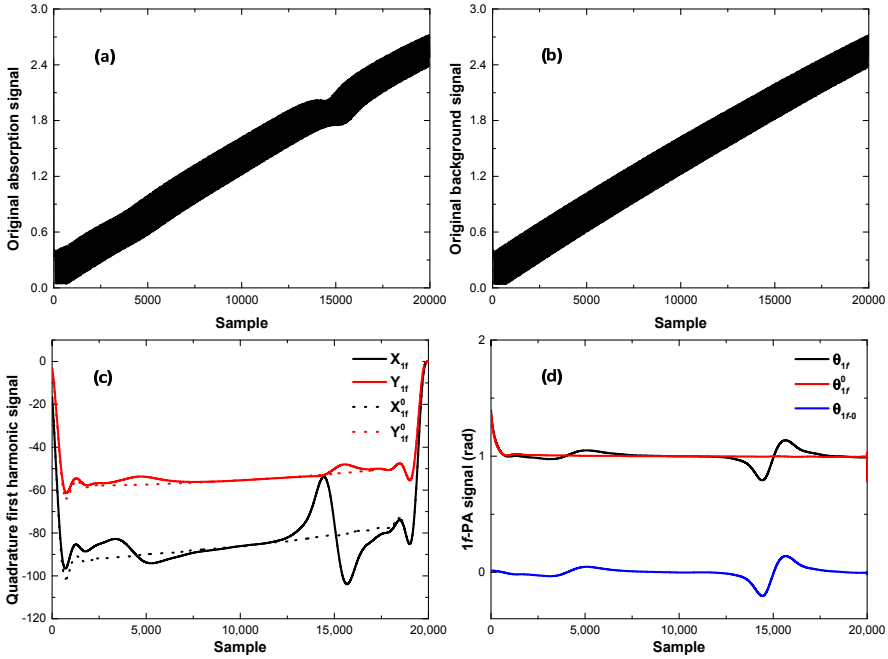

Figure 5. (a) the original absorption signal with high purity CO_2; (b) the original absorption signal with high purity N_2; (c) the absorption and background quadrature first-harmonic signals; (d) the absorption and background 1*f*-PAs and the background subtracted 1*f*-PA.

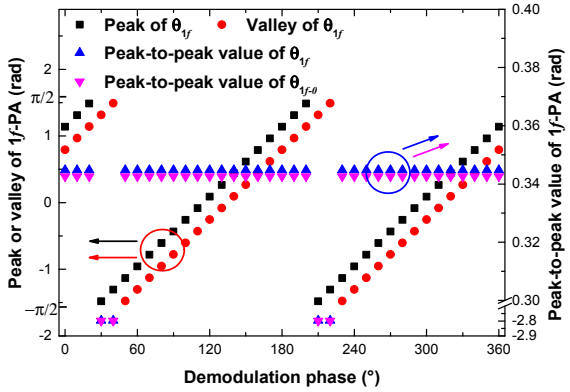

Fig. 6. The peak, valley, and peak-to-peak values with different demodulation phases.

3.3 First harmonic phase angles with different modulation parameters

The peak-to-peak values of the background subtracted 1*f*-PA ($\theta_{1f\text{-}0}$) under different modulation amplitudes and frequencies were measured with pure CO_2 to investigate the feasibility of the 1*f*-PA method for gas concentration retrieval. The measurement results were also compared with the peak values of the root-sum-square magnitude of the background

Optics EXPRESS

subtracted *2f/1f* signals ($R_{2f/1f\text{-}0}$). Demodulation parameters are the same with those used in Section 3.2. The maximum modulation amplitude is limited by the ramp current and the maximum inject current of the laser, and the maximum modulation frequency is limited by the sample rate of the I/O device.

The FM amplitude and IM-FM phase shift of the DFB laser diode used in this paper are measured with the etalon. The modulation index m is calculated by dividing the FM amplitude by the self-broadened HWHM of CO_2 under 1 atm pressure. As shown in Fig. 7(a), the FM amplitude linearly increases with the modulation current, but decreases with the increasing of the modulation frequency. This implies that the best modulation index (m = 1.1) for 2*f*/1*f* signals cannot be achieved when the modulation frequency is higher than 40 kHz. The IM-FM phase shift increases with the increasing of the modulation frequency, and almost remains constant for different modulation amplitudes.

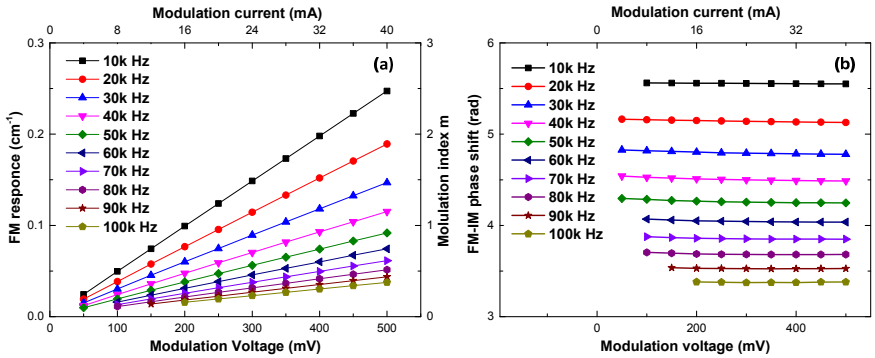

Fig. 7. Frequency amplitude (a) and IM-FM phase shift (b) of the DFB laser diode with different modulation currents and frequencies.

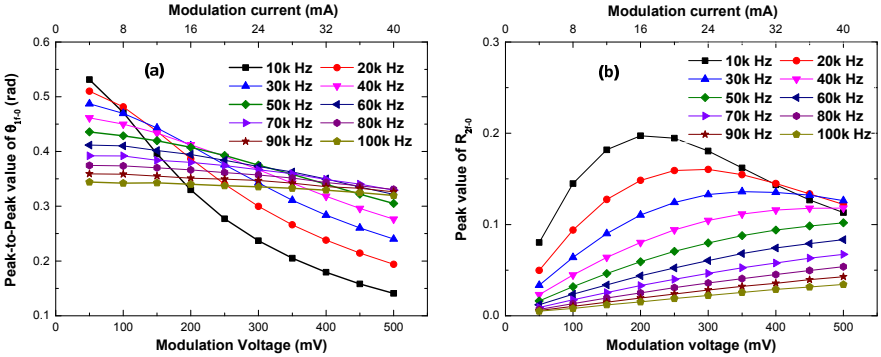

Fig. 8. Peak-to-peak values of $\theta_{1f\text{-}0}$ (a) and peak values of $R_{2f/1f\text{-}0}$ (b) for pure CO_2 with different modulation currents and frequencies.

The peak-to-peak values of $\theta_{1f\text{-}0}$ and the peak values of $R_{2f/1f\text{-}0}$ are plotted in Fig. 8. The local maximum of the peak values of $R_{2f/1f\text{-}0}$ appears at 16 mA (200 mV) modulation amplitude for 10 kHz modulation frequency. However, the modulation amplitude of the $R_{2f/1f\text{-}0}$ local maximum continuously increases with the increasing of the modulation frequency. Unlike the peak value of $R_{2f/1f\text{-}0}$, the peak-to-peak value of $\theta_{1f\text{-}0}$ decreases with the modulation amplitude monotonously, especially at low modulation frequencies. At high modulation frequencies, the peak-to-peak value of $\theta_{1f\text{-}0}$ is not sensitive to modulation amplitude, because of the low FM response ratio. As mentioned in Section 2, $\theta_{1f\text{-}0}$ can be approximately estimated

Optics EXPRESS

by the ratio between the modulus of the sum of absorption-related vectors and the modulus of the 1*f* RAM vector, which is linearly proportional to the IM amplitude. Therefore, $\theta_{1f\text{-}0}$ decreases with the increasing of the modulation amplitude. However, this does not imply that small modulation amplitude should be chosen, as the signal-to-noise ratio of the absorption signals also deteriorates with the decreasing of the modulation amplitude due to the presence of various noises. After all, the modulation amplitude should be optimized to achieve the best SNR for $\theta_{1f\text{-}0}$ rather than the maximum value. On the other hand, the influence of the FM-IM phase shift is notable at small modulation amplitude. At 4 mA (50 mV) modulation amplitude, the peak-to-peak value of $\theta_{1f\text{-}0}$ decreases with the modulation frequency due to the increasing of the FM-IM phase shift.

3.4 Linearity and sensitivity of first harmonic phase angles

Experiments with a series of concentrations of CO_2 balanced by N_2 that varies with two orders of magnitude from 0 to 80% were performed to verify the linearity of the 1*f*-PA method. The peak-to-peak values of $\theta_{1f\text{-}0}$ and the peak values of $R_{2f/1f\text{-}0}$ show good correlations with the CO_2 concentration particularly at the high modulation frequency, as illustrated in Fig. 9. The correlation coefficient is generally better than 0.99 for both methods. The stability of the 1*f*-PA method has also been compared with the traditional 2*f*/1*f* method by employing the Allen deviation. Figure 10 shows the Allen deviations of CO_2 mole fraction retrieved by peak-to-peak values of $\theta_{1f\text{-}0}$ and peak values of $R_{2f/1f\text{-}0}$. For the low modulation frequency (10 kHz), the two techniques have similar stabilities. However, the Allen deviation of $\theta_{1f\text{-}0}$ at the high modulation frequency (100 kHz) has similar performance as that measured at the low modulation frequency, while the Allen deviation of $R_{2f/1f\text{-}0}$ significantly deteriorates with the increasing of the modulation frequency.

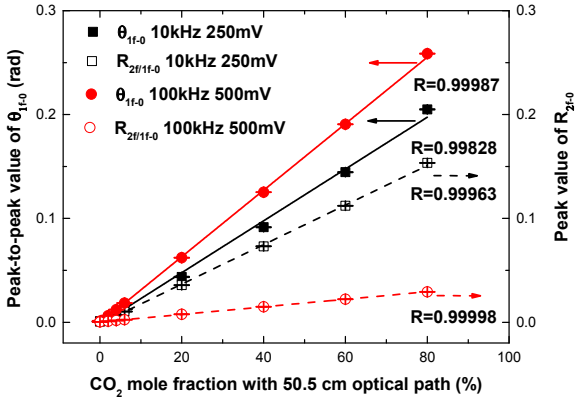

Fig. 9. Peak-to-peak values of $\theta_{1f\text{-}0}$ and peak values of $R_{2f/1f\text{-}0}$ as a function of CO_2 concentration with different modulation amplitudes and frequencies.

Optics EXPRESS

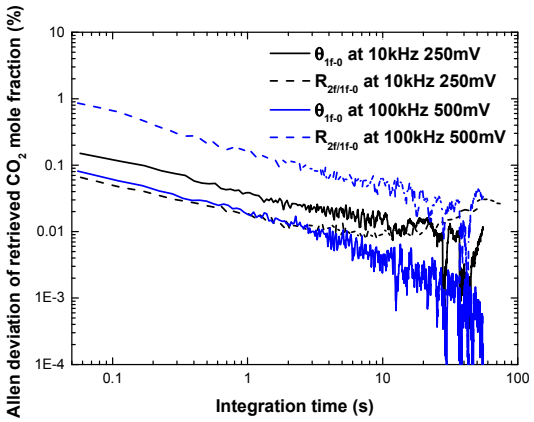

Fig. 10. Allen deviation of retrieved CO_2 mole fraction by peak-to-peak values of $\theta_{1f\text{-}0}$ and peak values of $R_{2f/1f\text{-}0}$.

Table 1 shows the correlation coefficient and the Allen Deviation measured with different modulation parameters and 1-s integration time. As has been discussed above, the correlation coefficient of $\theta_{1f\text{-}0}$ slightly improves with the increasing of the modulation frequency. The Allen deviations of $\theta_{1f\text{-}0}$ and $R_{2f/1f\text{-}0}$ decrease simultaneously with the increasing of the modulation current. By increasing the modulation frequency from 10 kHz to 100 kHz, the Allen deviation of $\theta_{1f\text{-}0}$ keeps the same level, about 2 ppm within 1-s integration time, while the Allen deviation of $R_{2f/1f\text{-}0}$ is one order of magnitude worse.

Table 1. Correlation coefficient and Allen variance of $\theta_{1f\text{-}0}$ and $R_{2f/1f\text{-}0}$

Modulation condition	Correlation coefficient		Allen deviation(ppm@1s)	
	$\theta_{1f\text{-}0}$	$R_{2f/1f\text{-}0}$	$\theta_{1f\text{-}0}$	$R_{2f/1f\text{-}0}$
10 kHz 250 mV	0.9983	0.9991	2.17	1.88
10 kHz 500 mV	0.9985	0.9989	1.91	1.36
50 kHz 250 mV	0.9997	0.9995	1.99	5.62
50 kHz 500 mV	0.9993	0.9999	1.12	2.04
100 kHz 250 mV	0.9998	0.9998	3.85	72.49
100 kHz 500 mV	0.9999	1.0000	1.83	14.85

4. Conclusion

In this paper, the 1*f*-PA method, which is immune to the variances of signal intensity and demodulation phase, is proposed and validated for WMS measurements. The 1*f*-PA is approximately linearly dependent on the integral absorption under weak absorption conditions. The principle has been verified by measuring the CO_2 absorption around 6362.5 cm^{-1} with a near infrared DFB diode laser. The relationship between the peak-to-peak value of $\theta_{1f\text{-}0}$ and modulation parameters is carefully studied. The peak-to-peak value of $\theta_{1f\text{-}0}$ decreases with the modulation amplitude monotonously. The relationship between the peak-to-peak value of $\theta_{1f\text{-}0}$ and the modulation frequency is complicated due to the influence of the laser FM response ratio and the IM-FM phase shift. Finally, the linearity and sensitivity of the 1*f*-PA method are compared with the traditional 2*f*/1*f* method for different modulation conditions. The correlation coefficients with the CO_2 concentrations are generally better than 0.998 for these two methods and their Allen Variances are also similar for low modulation frequencies. Nevertheless, the sensitivity of the 1*f*-PA method nearly stays the same with the increasing of the modulation frequency, while the sensitivity of the traditional 2*f*/1*f* method deteriorates significantly. Overall, the 1*f*-PA method shows better performance than the traditional 2*f*/1*f* method under high modulation frequencies or modulation depth limited conditions, such as strong turbulence or high pressure environments.

Optics EXPRESS

Funding

National Key R&D Program of China (2017YFC0804900, 2016YFC0201100, 2016YFC0200600); Natural National Science Foundation of China (NSFC) (61805286, 61705030).

References

1. H. Nasim and Y. Jamil, "Recent advancements in spectroscopy using tunable diode lasers," Laser Phys. Lett. **10**(4), 043001 (2013).
2. K. Song and E. C. Jung, "Recent developments in modulation spectroscopy for trace gas detection using tunable diode lasers," Appl. Spectrosc. Rev. **38**(4), 395–432 (2003).
3. P. Geiser, "New opportunities in mid-infrared emission control," Sensors (Basel) **15**(9), 22724–22736 (2015).
4. C. Wang and P. Sahay, "Breath analysis using laser spectroscopic techniques: breath biomarkers, spectral fingerprints, and detection limits," Sensors (Basel) **9**(10), 8230–8262 (2009).
5. S. Reuter, J. S. Sousa, G. D. Stancu, and J.-P. Hubertus van Helden, "Review on VUV to MIR absorption spectroscopy of atmospheric pressure plasma jets," Plasma Sources Sci. Technol. **24**(5), 054001 (2015).
6. G. Galbács, "A review of applications and experimental improvements related to diode laser atomic spectroscopy," Appl. Spectrosc. Rev. **41**(3), 259–303 (2006).
7. P. Kluczynski, J. Gustafsson, Å. M. Lindberg, and O. Axner, "Wavelength modulation absorption spectrometry — an extensive scrutiny of the generation of signals," Spectrochim. Acta B At. Spectrosc. **56**(8), 1277–1354 (2001).
8. S. Schilt, L. Thévenaz, and P. Robert, "Wavelength modulation spectroscopy: combined frequency and intensity laser modulation," Appl. Opt. **42**(33), 6728–6738 (2003).
9. H. Li, G. B. Rieker, X. Liu, J. B. Jeffries, and R. K. Hanson, "Extension of wavelength-modulation spectroscopy to large modulation depth for diode laser absorption measurements in high-pressure gases," Appl. Opt. **45**(5), 1052–1061 (2006).
10. C. S. Goldenstein, C. L. Strand, I. A. Schultz, K. Sun, J. B. Jeffries, and R. K. Hanson, "Fitting of calibration-free scanned-wavelength-modulation spectroscopy spectra for determination of gas properties and absorption lineshapes," Appl. Opt. **53**(3), 356–367 (2014).
11. G. Zhao, W. Tan, J. Hou, X. Qiu, W. Ma, Z. Li, L. Dong, L. Zhang, W. Yin, L. Xiao, O. Axner, and S. Jia, "Calibration-free wavelength-modulation spectroscopy based on a swiftly determined wavelength-modulation frequency response function of a DFB laser," Opt. Express **24**(2), 1723–1733 (2016).
12. L. Tao, K. Sun, D. J. Miller, M. A. Khan, and M. A. Zondlo, "Current and frequency modulation characteristics for continuous-wave quantum cascade lasers at 9.06 μm," Opt. Lett. **37**(8), 1358–1360 (2012).
13. L. Mei and S. Svanberg, "Wavelength modulation spectroscopy--digital detection of gas absorption harmonics based on Fourier analysis," Appl. Opt. **54**(9), 2234–2243 (2015).
14. P. Zhimin, D. Yanjun, C. Lu, and Y. Qiansuo, "Odd harmonics with wavelength modulation spectroscopy for recovering gas absorbance shape," Opt. Express **20**(11), 11976–11985 (2012).
15. A. Hangauer, J. Chen, R. Strzoda, and M.-C. Amann, "Multi-harmonic detection in wavelength modulation spectroscopy system," Appl. Phys. B **110**(2), 177–185 (2013).
16. L. Lan, Y. Ding, Z. Peng, Y. Du, Y. Liu, and Z. Li, "Multi-harmonic measurements of line shape under low absorption conditions," Appl. Phys. B **117**(2), 543–547 (2014).
17. G. Stewart, W. Johnstone, J. R. P. Bain, K. Ruxton, and K. Duffin, "Recovery of absolute gas absorption line shapes using tunable diode laser spectroscopy with wavelength modulation—part 1: theoretical analysis," J. Lightwave Technol. **29**(6), 811–821 (2011).
18. J. R. P. Bain, W. Johnstone, K. Ruxton, G. Stewart, M. Lengden, and K. Duffin, "Recovery of absolute gas absorption line shapes using tunable diode laser spectroscopy with wavelength modulation—part 2: experimental investigation," J. Lightwave Technol. **29**(7), 987–996 (2011).
19. A. J. McGettrick, K. Duffin, W. Johnstone, G. Stewart, and D. G. Moodie, "Tunable diode laser spectroscopy with wavelength modulation: a phasor decomposition method for calibration-free measurements of gas concentration and pressure," J. Lightwave Technol. **26**(4), 432–440 (2008).
20. K. Duffin, A. J. McGettrick, W. Johnstone, G. Stewart, and D. G. Moodie, "Tunable diode-laser spectroscopy with wavelength modulation: a calibration-free approach to the recovery of absolute gas absorption line shapes," J. Lightwave Technol. **25**(10), 3114–3125 (2007).
21. A. Upadhyay and A. L. Chakraborty, "Calibration-free 2f WMS with in situ real-time laser characterization and 2f RAM nulling," Opt. Lett. **40**(17), 4086–4089 (2015).